

# Decentralized Automotive Radar Spectrum Allocation to Avoid Mutual Interference Using Reinforcement Learning

Pengfei Liu, Yimin Liu<sup>\*</sup>, *Member, IEEE*, Tianyao Huang, Yuxiang Lu, and Xiqin Wang

**Abstract**—Nowadays, mutual interference among automotive radars has become a problem of wide concern. In this paper, a decentralized spectrum allocation approach is presented to avoid mutual interference among automotive radars. To realize decentralized spectrum allocation in automotive scenarios meet with two challenges: 1) the allocation approach should be dynamic due to the changing positions of all radars; 2) each radar has no communication with others so it has quite limited information. A machine learning technique, reinforcement learning (RL), is utilized because RL can learn a decision making policy in an unknown dynamic environment. As radar’s single observation is incomplete, a long short-term memory (LSTM) recurrent network is used to aggregate radar’s observations through time so that a subband is chosen by combining both the present and past observations. Simulation experiments are conducted to compare the proposed approach with other common spectrum allocation methods such as the random and myopic policy, showing that our approach outperforms the others.

**Index Terms**—automotive radar, interference, spectrum allocation, reinforcement learning

## I. INTRODUCTION

Nowadays, people’s pursuit for safe and comfortable driving gives rise to more and more self-driving technologies, such as adaptive cruise control (ACC) and collision warning (CW). Automotive radar, as one of the most important sensors on vehicles, is vastly popularized. In most countries, the frequency range of 76-77 GHz is allocated to automotive usage [1]. As the population and bandwidth demand of automotive radars are both on the rise, mutual interference becomes a problem of wide concern.

Frequency modulated continuous wave (FMCW) is widely employed in automotive radar due to its low hardware complexity [2]. The consequences of mutual interference among FMCW radars have been investigated in [1, 3–6]. The probability of ghost targets is raised if an FMCW radar is interfered by another with the same chirp rate [1, 3, 4]. To prevent ghost targets, [5] proposed to use random chirp rates so that interference resulted in an elevation of the noise level. Such interference is referred to as non-coherent interference in [6]. The MOSARIM project also concluded that the most probable

consequence of real-world automotive radar interference was to increase the receiver noise which might cover targets [7].

Current solutions to mitigating automotive radar interference can be grouped into two genres, interference canceling (IC) and interference avoidance (IA). IC techniques are usually applied in the radar receiver to eliminate interference from the received signal, e.g. [8–11], while IA is to coordinate transmission in time domain, frequency domain and space domain, etc, to prevent interference from occurring [12]. A representative IA method in the frequency domain is spectrum allocation. For example, [13] describes a method in which the whole band is divided into several non-overlapping subbands based on resolution requirement. Then, radars are assigned to different subbands so they do not interfere with each other. However, it will suffer performance degradation in avoiding interference when radars are more than subbands. In [14], a centralized spectrum allocation scheme is proposed. Each radar sends information including its own position and velocity to a control center, which computes the allocation results and then broadcasts them to each radar. However, it increases extra communication cost. By contrast, in decentralized allocation, each radar chooses frequency bands in an autonomous way. A common method is to choose at random [14], which is easy to implement but has limited performance improvement.

In this paper, we present an IA approach for FMCW automotive radar by decentralized spectrum allocation. In our approach, we also assume that the whole band is divided into several non-overlapping subbands, given radar’s resolution or bandwidth requirement. Moreover, we consider the cases where radars are more than subbands. Based on the premise, we propose a decentralized spectrum allocation approach in which each radar chooses a subband separately to reduce the mutual interference. Although decentralized spectrum allocation has been extensively studied in cognitive radio sensor networks, in automotive scenarios it meet with two challenges. First, the allocation approach should be dynamic as all radars are mounted on moving vehicles. Second, each radar does not communicate with others so it has quite limited information. In light of these challenges, a machine learning technique, reinforcement learning (RL), is employed since RL can learn a decision making policy in an unknown dynamic environment. Moreover, a long short-term memory (LSTM) recurrent network is utilized to aggregate radar’s observations through time so that a subband is chosen by combining both the present and past observations.

RL has been successfully applied to related areas, such as

P. Liu, Y. Liu, T. Huang and X. Wang are with the Department of Electronic Engineering, Tsinghua University, Beijing, China (e-mail: liupf16@mails.tsinghua.edu.cn; yiminliu@tsinghua.edu.cn; huang-tianyao@tsinghua.edu.cn; wangxq\_ee@tsinghua.edu.cn).

Y. Lu is with Beijing Radar Research Institute, Beijing, China (email: luyuxiang92@163.com).

<sup>\*</sup>Corresponding author.

cognitive radar (CR) [15–17] and dynamic spectrum access (DSA) [18–23] in communication. CR was firstly proposed in [24], which established a closed-loop mode and feedback facility between radar transmitter and receiver for a better adaption to the changing environment. In this sense, the automotive radar in our problem is cognitive because the transmitter adaptively chooses subbands according to the receiver's observations on the environment. Recently, CR and RL have been merged to solve problems in cognitive electronic warfare (CEW) [15, 17] and waveform optimization [16]. However, only a single radar is considered in these researches. In this work, we apply RL to a multi-radar interference avoiding problem in which each automotive radar cognitively changes subbands according to their observations.

Multi-user interference problem is also examined in DSA, in which a channel/subband access policy is developed so that each user can avoid collisions with others. In DSA, different RL techniques have been implemented, such as traditional Q-learning [18, 19] and deep RL [21–23], in which neural networks are used to represent the Q-function. Various network types have been adopted, such as multi-layer perceptrons (MLP) [22, 23] and recurrent neural networks (RNN) [21]. In these DSA researches [18, 19, 21–23], users are assumed to be static. However, in our problem, radars are mounted on moving vehicles, so the radio environment changes with radars' positions. To cope with such situation, first, we address how radar acquires the position-related observations, which include not only the detected range of other radars, but also the estimated interference power. Then, we show how radar exploits these observations to choose a proper subband.

To sum up, the main contributions of this paper are listed as follows.

- A decentralized spectrum allocation approach for automotive radar is proposed using RL. Each radar learns to choose a subband to avoid interference according to its own observations, with no communication required.
- The LSTM network is utilized in the RL-based spectrum allocation approach so that radar can choose a subband by combining its current and past observations. Moreover, an algorithm to train the LSTM network in our problem is put forward.
- Simulation experiments are conducted to compare the proposed approach with other common decentralized spectrum allocation methods such as the random and myopic policy, showing that our approach outperforms the others.

The rest of the paper is organized as follows. In Section II, the scenario and signal model are constructed. In Section III, how radar measures the range, velocity and interference is described. In Section IV, the decentralized spectrum allocation approach using RL with LSTM network is elaborated. Simulation results and concluding remarks are presented in Section V and VI, respectively.

## II. SCENARIO AND SIGNAL MODEL

A simplified scenario considered in our problem is shown in Fig. 1, in which cars are traveling in two lanes with different

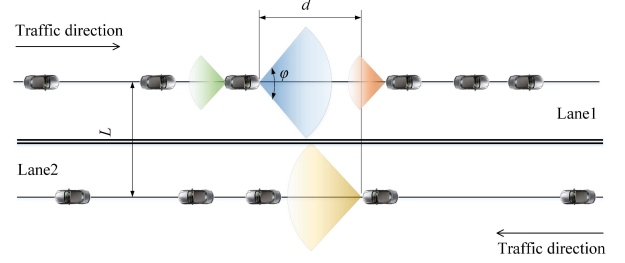


Fig. 1. Problem scenario.

traffic directions. Each car is equipped with one long-range radar (LRR) on its front and one short range radar (SRR) on its back. The LRR is used to provide a forward-looking view for applications such as adaptive cruise control (ACC) and collision mitigation systems (CMS) [25]. The SRR is used to detect obstacles for applications such as lane change assistance (LCA) and assisted parking system (APS) [25].

As is mentioned in the previous section, it is presumed that the whole band is equally divided into  $M$  non-overlapping subbands. Suppose there are  $N$  cars on a certain section of the road and they are indexed by  $1, 2, \dots, N$ . Every time interval  $T$ , a car chooses a working subband for both the LRR and SRR. As subbands are fewer than radars, i.e.  $N > M$ , more than one radars will inevitably collide into the same subband causing interference. In this paper, we only focus on reducing LRR interference, as SRR interference is usually not a concern [5].

In this work, the commonly used triangular chirp FMCW waveform [5, 14] is employed in each automotive radar. The transmitted waveform is

$$s(t) = \begin{cases} \exp\left(j\pi\frac{B}{T_c}t^2\right) \exp(j2\pi f_m t) & 0 \leq t < T_c \\ \exp\left(-j\pi\frac{B}{T_c}(t-2T_c)^2\right) \exp(j2\pi f_m t) & T_c \leq t < 2T_c \end{cases}, \quad (1)$$

where  $T_c$  is the chirp interval and  $f_m = f_0 + mB$  is the carrier frequency for the  $m$ th subband. The chirp interval determines the chirp rate as the bandwidth of each subband is constant. In this work, to avoid ghost targets, radars on different cars use different chirp rates. Fig. 2 shows two chirps with different chirp rates.

The received signal is composed of the target echo, interference and noise:

$$r(t) = e(t) + h(t) + n(t), \quad (2)$$

where  $e(t)$ ,  $h(t)$  and  $n(t)$  denote the echo, interference and noise, respectively.

The echo from a single target is a delayed version of the transmitted signal:

$$e(t) = \sqrt{P_S} \cdot s(t - \tau(t)), \quad (3)$$

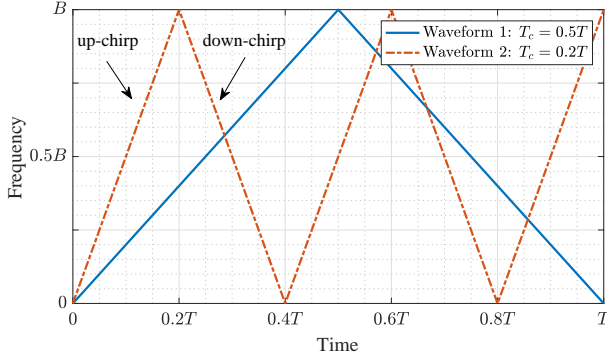


Fig. 2. Instantaneous frequency of two chirps with different chirp rates.

where  $P_S$  is the received signal power and  $\tau(t)$  the time delay of the target reflection. For an approaching target with relative radial velocity  $v$ ,

$$\tau(t) = \frac{2(R - vt)}{c}, \quad (4)$$

where  $R$  is the target radial distance and  $c$  the light speed.

Likewise, the received interference signal from another radar with transmitted signal  $s'(t)$  is

$$h(t) = \sqrt{P_I} \cdot s'(t - \tau'(t)), \quad (5)$$

where  $P_I$  is the received interference power and  $\tau'(t)$  the time delay:

$$\tau'(t) = \frac{(R' - v't)}{c}, \quad (6)$$

where  $R'$  is the the radial distance and  $v'$  the relative radial velocity of the interfering radar.

The received interference power  $P_I$  depends on the relative positions of the two radars. If they are located on different lanes (indicating the interfering radar is an LRR),

$$P_I = \frac{P_L G A_e g}{4\pi(L^2 + d^2)} \cdot [p_r(\theta(d))]^2, \quad (7)$$

where

- $P_L$ : transmitting power of LRR;
- $G$ : antenna gain;
- $A_e$ : effective area;
- $L$ : vertical distance between two lanes;
- $d$ : horizontal distance between two radars;
- $\theta$ : radiation direction between two radars;
- $p_r(\cdot)$ : normalized antenna beam pattern;
- $g$ : propagation decaying factor.

In (7), the antenna pattern  $p_r(\cdot)$  is taken into consideration, which indicates that the transmitting or receiving power also depends on the direction from one radar to another. An illustration of the antenna pattern is provided in Fig. 3. The direction can be written as a function of  $d$ :

$$\theta(d) = \arctan\left(\frac{L}{d}\right). \quad (8)$$

If the two radars are located on the same lane (indicating the interfering radar is an SRR),

$$P_I = \frac{P_S G A_e g}{4\pi d^2}, \quad (9)$$

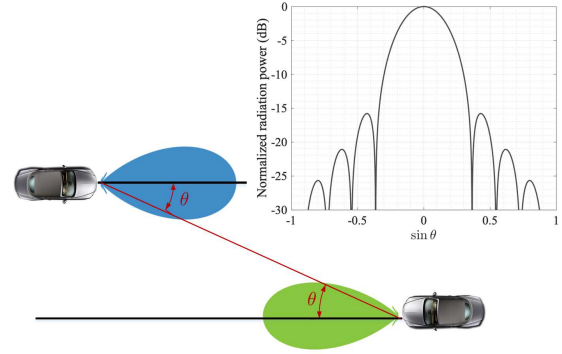


Fig. 3. Illustration of radar antenna pattern.

where  $P_S$  is the SRR transmitting power. The antenna pattern is omitted here because the direction is approximately 0.

### III. RADAR MEASUREMENT

#### A. Range and Velocity

The range and velocity information is extracted by analyzing the frequency difference, which is referred to as the beat frequency [3], between the transmitted and received signal. The beat frequency of the up-chirp and down-chirp can be expressed as [5]

$$f_b^\uparrow \approx \frac{B}{T_c} \cdot \frac{2R}{c} - \frac{2v}{c} f_m \quad (10)$$

$$f_b^\downarrow \approx -\frac{B}{T_c} \cdot \frac{2R}{c} - \frac{2v}{c} f_m, \quad (11)$$

respectively. The two beat frequencies can be estimated by analyzing the frequency spectrum of the received signal, which is expressed as

$$R(f) = \mathcal{F}\{s(t) \cdot \bar{r}(t)\}, \quad (12)$$

where  $\mathcal{F}$  represents Fourier transformation and  $\bar{r}(t)$  is the conjugate of  $r(t)$ . Then, the range and velocity can be calculated according to (10)(11).

#### B. Interference

If the working radar and the interfering radar use the same chirp rates, it will result in ghost targets as constant beat frequencies will be generated in the working radar's receiver. Ghost targets may mask true targets because interference is usually much stronger than echoes. To prevent ghost target, we assume that each car exploits a different chirp rate from one another. In this way, the frequency difference between two chirps is not constant but sweeps across the subband. Instead of resulting in ghost targets, it will raise the noise level. Fig. 4 illustrates the cases of no interference, ghost targets and raised noise level, respectively.

In cases where two radars uses different chirp rates, the interference power can be measured by the noise level, which is defined as:

$$N_I = \int |H(f) + N(f)|^2 df, \quad (13)$$

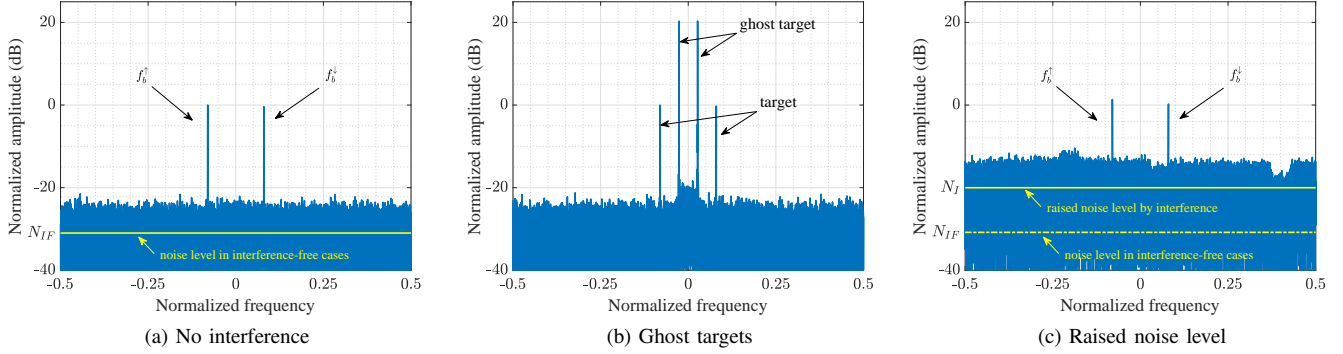


Fig. 4. Consequences of three cases where an FMCW chirp radar is (a) not interfered; (b) interfered by another radar with the same chirp rate; (c) interfered by another radar with a different chirp rate.

where

$$H(f) = \mathcal{F}\{r(t) \cdot \bar{h}(t)\} \quad (14)$$

$$N(f) = \mathcal{F}\{r(t) \cdot \bar{n}(t)\}. \quad (15)$$

The problem is to estimate  $N_I$  using the spectrum of the received signal,  $R(f)$ , which also contains echoes from targets. Some robust estimation techniques have been developed to solve similar problems. For instance, in [26], ordered statistics (OS) is used to estimate the clutter power in existence of heterogeneous samples. Likewise, we use OS to estimate the noise level. By sampling  $S(f)$  with a sampling interval  $\Delta f$ , we obtain a sequence  $\{R_m\} (0 \leq m \leq M_f - 1)$ , where  $M_f$  is the sequence length. Then, by sorting the sequence according to decreasing amplitude, we obtain a new one:

$$|R_{(0)}| \geq |R_{(1)}| \geq \dots \geq |R_{(M_f-1)}|. \quad (16)$$

Then, the noise level is estimated by leaving out the greatest  $K$  samples:

$$\hat{N}_I = \sum_{m=K}^{M_f-1} |R_{(m)}|^2 \Delta f. \quad (17)$$

Denote the interference-free noise level as  $N_{IF}$ , which is related to the receiver noise power and can be regarded as known. Then, the relative noise level is defined as

$$\eta = \frac{\hat{N}_I}{N_{IF}}. \quad (18)$$

In Fig. 5, we plot the relative noise level versus the interference-to-noise ratio (INR). The INR is defined as

$$\text{INR} = \frac{P_I}{\sigma^2}, \quad (19)$$

where  $\sigma^2$  is the receiver noise power. At each value of INR, we simulate 10 cases where two radars randomly select two different chirp rates. Fig. 5 conveys two messages: 1)  $\eta$  increases nearly linearly with INR; 2)  $\eta$  is almost irrelevant to different combinations of chirp rates. Therefore, the relative noise level  $\eta$  can be used as a metric for the interference power in our problem.

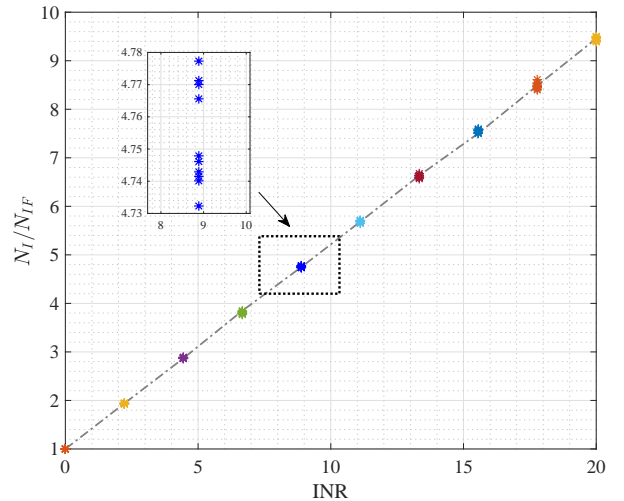


Fig. 5. Relative noise level versus INR. At each value of INR, we simulate 10 cases where two radars randomly select two different chirp rates. The inner subfigure is a magnified version of the plot within the dashed box.

#### IV. SPECTRUM ALLOCATION USING RL

The outline of the RL-based spectrum allocation approach for automotive radar is shown in Fig. 6. First, by processing the received signal from last time step, the receiver constructs the current observation  $\mathbf{o}_t$ . The construction of  $\mathbf{o}_t$  will be described in detail in Subsection IV.A. Then, the transmitter employs a Q-network to choose a subband  $u_t$  by aggregating the historical observations  $\{\mathbf{o}_t, \mathbf{o}_{t-1}, \dots, \mathbf{o}_1\}$ . In the meantime, the receiver also gives feedback to the transmitter in the form of a reward signal  $r_{t-1}^i$ , which is evaluated based on the relative noise level  $\eta_{t-1}^i$ . The reward acts as a tutor guiding the Q-network to adjust parameters to generate a better subband selecting policy.

##### A. Reward and Receiver Observation

The reward is defined in terms of the relative noise level  $\eta_t^i$ . If  $\eta_t^i$  is below a predefined threshold  $\eta_0$ , the transmission

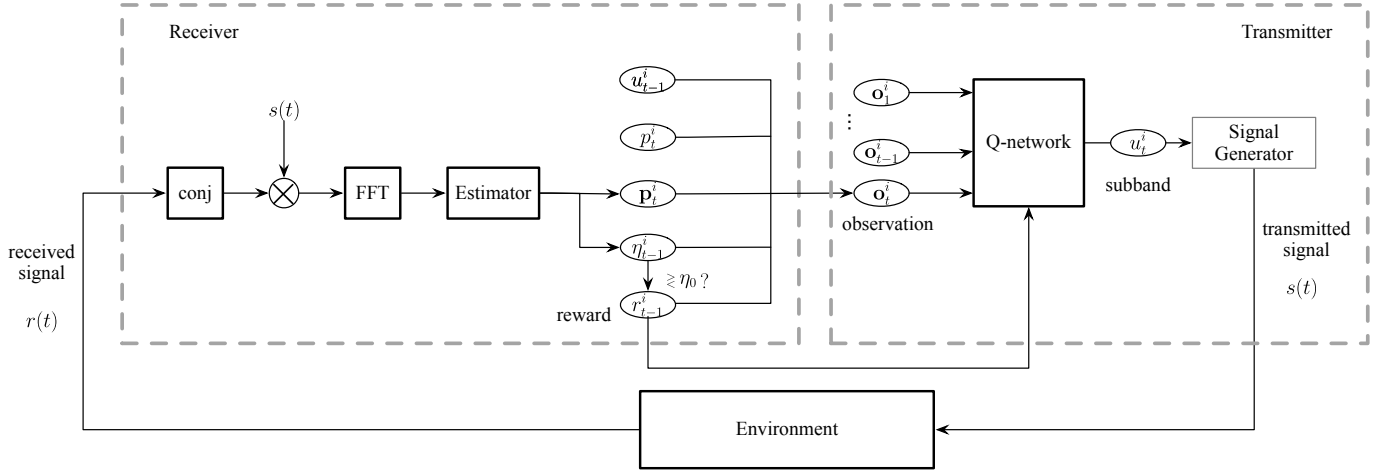


Fig. 6. Outline of the RL-based spectrum allocation approach for automotive radar.

is regarded as successful and the corresponding reward is 1; otherwise, the reward is 0, i.e.

$$r_t^i = \begin{cases} 1 & \eta_t^i < \eta_0 \\ 0 & \eta_t^i \geq \eta_0 \end{cases}. \quad (20)$$

The observation which Car  $i$  acquires at time step  $t$  is

$$\mathbf{o}_t^i = [u_{t-1}^i, r_{t-1}^i, \eta_{t-1}^i, p_t^i, \mathbf{p}_t^i], \quad (21)$$

where

- $u_{t-1}^i$ : the last subband which Car  $i$  transmitted;
- $r_{t-1}^i$ : the last reward which Car  $i$  received;
- $\eta_{t-1}^i$ : the relative noise level in last time step;
- $p_t^i$ : the position of Car  $i$ ;
- $\mathbf{p}_t^i$ : the estimated positions of cars in front of Car  $i$ .

The car's own position  $p_t^i$  can be acquired from its onboard sensors such as GPS and INS. The estimated position  $\mathbf{p}_t^i$  is a two dimensional vector:

$$\mathbf{p}_t^i = [p_{S,t}^i, p_{D,t}^i], \quad (22)$$

where  $p_{S,t}^i, p_{D,t}^i$  are the position of the nearest car in front of Car  $i$  in the same and different lane, respectively. The vector  $\mathbf{p}_t^i$  is calculated according to radar's measurement of the range and velocity, which is accompanied with estimation errors caused by noise and interference.

### B. Q-network in Transmitter

In this subsection, first, we recap the RL and Q-learning algorithm. Then, we show how the Q-network is specified for the spectrum allocation problem.

In RL, an agent learns how to choose actions by receiving rewards from an unknown environment [27]. Let  $\mathbf{s}_t$ ,  $a_t$  and  $r_t$  denote the state of the environment, the action of the agent and the reward it receives at time step  $t$ . At each time step, action  $a_t$  is determined by environment state  $\mathbf{s}_t$  following a policy  $\pi$ , which is a mapping from the state space to the action space, by trying to maximize a discounted sum of future rewards:

$$G_t = r_t + \gamma r_{t+1} + \gamma^2 r_{t+2} + \dots, \quad (23)$$

where  $\gamma \in [0, 1]$  is the discounting factor. The factor  $\gamma$  reflects how much we consider the influence of the current action on the future. An extreme example is  $\gamma = 0$ , which corresponds to the case where the agent aims to maximize the immediate reward  $r_t$ . The Q-function is defined as the expectation of  $G_t$  after taking action  $a_t$  under environment state  $\mathbf{s}_t$  following policy  $\pi$ :

$$Q_\pi(\mathbf{s}_t, a_t) = \mathbb{E}\{G_t | \mathbf{s}_t, a_t, \pi\}, \quad (24)$$

where the expectation is taken over the probabilistic sequence,  $\mathbf{s}_{t+1}, a_{t+1}, r_{t+1}, \mathbf{s}_{t+2}, a_{t+2}, r_{t+2}, \dots$ , following policy  $\pi$ . Learning the optimal policy equals to finding the optimal Q-function:

$$Q^*(\mathbf{s}_t, a_t) = \max_{\pi} Q_\pi(\mathbf{s}_t, a_t). \quad (25)$$

Then, the best action can be determined by the optimal Q-function:

$$a_t^* = \arg \max_{a'} Q^*(\mathbf{s}_t, a'). \quad (26)$$

The Q-learning algorithm provides an iterative way to estimate the optimal Q-function even when an explicit model of the environment is unavailable. Each iteration is based on an experience of the agent, which is represented by a quadruple,  $(\mathbf{s}_t, a_t, r_t, \mathbf{s}_{t+1})$ . The iteration is performed as [27]:

$$Q(\mathbf{s}_t, a_t) \leftarrow Q(\mathbf{s}_t, a_t) + \alpha_t \left[ r_t + \gamma \max_{a'} Q(\mathbf{s}_{t+1}, a') - Q(\mathbf{s}_t, a_t) \right], \quad (27)$$

where  $\alpha_t$  is the learning step size. As the iteration in (27) is limited to cases where the state and action space are low dimensional and discrete, a neural network is usually used to approximate the Q-function [28]. The network is referred to as Q-network in the following.

In our problem, as  $\mathbf{s}_t$  is not fully observable, using a single observation to represent the environment state is inadequate. To construct a more complete environment state, the historical observations are aggregated:

$$\mathbf{s}_t^i = [\mathbf{o}_1^i, \mathbf{o}_2^i, \dots, \mathbf{o}_t^i], \quad (28)$$

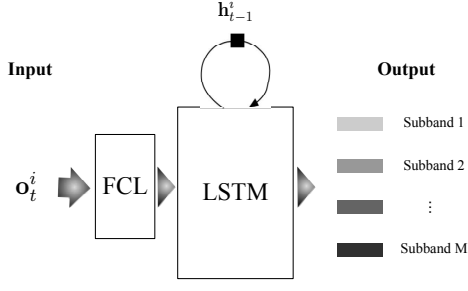


Fig. 7. The Q-network architecture. The black square stands for a time-step delay.

where  $s_t^i$  denotes the constructed environment state by Car  $i$ . Here, we use an LSTM recurrent neural network to approximate the Q-function since the LSTM structure is capable of memorizing the past by maintaining a hidden state [29]. The Q-network for Car  $i$  is denoted as  $Q^i(\mathbf{o}_t^i, \mathbf{h}_{t-1}^i, u_t^i; \mathbf{w}^i)$ , where  $\mathbf{w}^i$  is the network parameter,  $u_t^i$  is the chosen subband index by Car  $i$  at time step  $t$  and  $\mathbf{h}_{t-1}^i$  is the hidden state extracted from past observations  $\mathbf{o}_1^i, \mathbf{o}_2^i, \dots, \mathbf{o}_{t-1}^i$ . Using the LSTM network, the constructed environment state by Car  $i$  can be equally represented by:

$$\mathbf{s}_t^i = [\mathbf{o}_t^i, \mathbf{h}_{t-1}^i]. \quad (29)$$

The loss function of the  $i$ -th Q-network is defined as

$$\mathcal{L}^i(\mathbf{w}^i) = \mathbb{E} \left\{ \left( y_t^i - Q^i(\mathbf{o}_t^i, \mathbf{h}_{t-1}^i, u_t^i; \mathbf{w}^i) \right)^2 \right\}, \quad (30)$$

where the expectation is taken over each experience  $(\mathbf{o}_t^i, \mathbf{h}_{t-1}^i, u_t^i, r_t^i, \mathbf{o}_{t+1}^i, \mathbf{h}_t^i)$ , and  $y_t^i$  is the target value [27]:

$$y_t^i = r_t^i + \gamma \max_{u'} Q^i(\mathbf{o}_{t+1}^i, \mathbf{h}_t^i, u'; \mathbf{w}^{i-}), \quad (31)$$

where  $\mathbf{w}^{i-}$  represents the network parameters before the update. The loss function is to minimize the error between the Q-function and target values over experiences of all radars. Then, the gradient descent step is performed to finish the update:

$$\mathbf{w}^i = \mathbf{w}^{i-} - \beta \frac{\partial \mathcal{L}^i(\mathbf{w})}{\partial \mathbf{w}} \Big|_{\mathbf{w}=\mathbf{w}^{i-}}, \quad (32)$$

where  $\beta$  is the learning rate.

### C. Network Architecture

The Q-network architecture in our problem is shown in Fig. 7. A fully connected layer (FCL) transforms  $\mathbf{o}_t^i$  into inputs of the LSTM layers. The LSTM layers maintain a hidden state  $\mathbf{h}_{t-1}^i$ , which is extracted from past observations before time step  $t$ . Each element of the output represents the Q-function value of the corresponding subband. Fig. 8 shows the unfolded representation of the Q-network. At time  $t$ , subband  $u_t^i$  is chosen by combining the current observation  $\mathbf{o}_t^i$  and hidden state  $\mathbf{h}_{t-1}^i$ . Then  $\mathbf{h}_{t-1}^i$  evolves into  $\mathbf{h}_t^i$  by incorporating the new observation  $\mathbf{o}_t^i$ . In this way, the subband at each time step is determined by both the present and past observations.

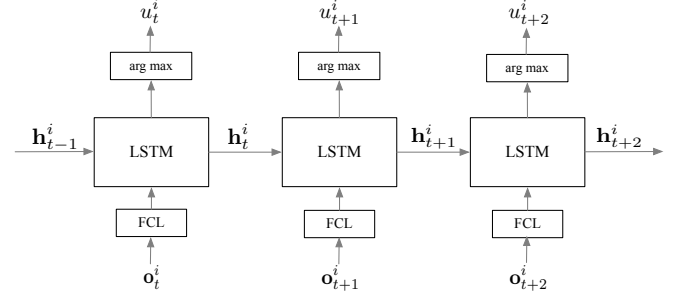


Fig. 8. Unfolded representation of the Q-network, showing a subband is determined by combining the present and past observations.

### D. Network Training

In this subsection, some details of the network training are given.

In the training, an episode refers to a succession of experiences starting from an initial state and ending after a certain number of time steps. In [30], several techniques are employed to train the deep Q-network with stability. In our problem, the following listed techniques are adopted with modifications to train the Q-network with recurrent structures.

- *Experience replay with batch learning.* During the training, each experience,  $e_t^i = (\mathbf{o}_t^i, \mathbf{h}_{t-1}^i, u_t^i, r_t^i, \mathbf{o}_{t+1}^i, \mathbf{h}_t^i)$ , is stored in memory. The memory only stores experiences of the recent 200 episodes. In each update, a batch of experiences are drawn from the memory. A batch is formed as (33) shows.

$$\left\{ \begin{array}{cccc} e_{t_1}^i & e_{t_1+1}^i & \cdots & e_{t_1+P-1}^i \\ e_{t_2}^i & e_{t_2+1}^i & \cdots & e_{t_2+P-1}^i \\ \vdots & \vdots & \ddots & \vdots \\ e_{t_K}^i & e_{t_K+1}^i & \cdots & e_{t_K+P-1}^i \end{array} \right\} \quad (33)$$

Each row in (33) is obtained following the two procedures: first, randomly picking an episode from the memory; then, randomly choosing a fraction which comprises of  $P$  successive experiences from the whole episode. The randomization among different rows improves training stability because it breaks the correlation of experience sequences [30].

- *$\epsilon$ -greedy policy.* At each time step, each car chooses a subband corresponding to the greatest Q-function value or otherwise a random one with small exploring probability  $\epsilon$ , i.e.

$$u_t^i = \begin{cases} \arg \max_{u'} Q^i(\mathbf{o}_t^i, \mathbf{h}_{t-1}^i, u'; \mathbf{w}^i) & a \geq \epsilon \\ \text{a random subband} & a < \epsilon \end{cases}, \quad (34)$$

where  $a$  is one realization of a uniformly distributed random variable ranged from 0 to 1.

- *Double networks.* For training stability, a separate network,  $\hat{Q}^i$ , is used to generate target values  $y_t^i$ . Every  $C$  time steps,  $\hat{Q}^i$  is replaced by the newly updated  $Q^i$ .

The Q-network training algorithm is summarized in Algorithm 1.

---

**Algorithm 1: Q-Network Training Algorithm**


---

```

1 Set up two set of networks,  $\{Q^i\}$  and  $\{\hat{Q}^i\}$ .
2 Initialize  $Q^i$  and  $\hat{Q}^i$  with the same random parameter  $\mathbf{w}^-$ .
3 for  $episode = 1 : N_e$  do
4   Initialize hidden state  $\mathbf{h}_0^i$  and observation  $\mathbf{o}_1^i$ ,
    $\forall i \in \{1, 2, \dots, N\}$ .
5   for  $t = 1 : T$  do
6     for  $Car\ i = 1 : N$  do
7       Feed observation  $\mathbf{o}_t^i$  to network  $\mathbf{Q}^i$  to get a
       set of action values
        $\{Q^i(\mathbf{o}_t^i, \mathbf{h}_{t-1}^i, u; \mathbf{w})\} (u = 1, 2, \dots, M)$  and
       the hidden state  $\mathbf{h}_t^i$ .
8       Choose a subband  $u_t^i$  as (34).
9       Get a reward  $r_t^i$ .
10      Obtain new observation  $\mathbf{o}_{t+1}^i$ 
11      Store  $e_t^i = (\mathbf{o}_t^i, \mathbf{h}_{t-1}^i, u_t^i, r_t^i, \mathbf{o}_{t+1}^i, \mathbf{h}_t^i)$  into
       memory.
12      Form a batch as (33).
13      Calculate target values  $y_t^i$  using network  $\hat{Q}^i$ .
14       $\mathbf{w}^i \leftarrow \mathbf{w}^i - \beta \frac{\partial \mathcal{L}^i(\mathbf{w})}{\partial \mathbf{w}}$ .
15      Every  $C$  time steps,  $\hat{Q}^i = Q^i$ .
16    end
17  end
18 end

```

---

## V. SIMULATIONS

In this section, simulations results are presented to verify the proposed approach. In the following, first, the simulation setup is described. Then, two contrasting approaches are introduced. Last, simulation results along with corresponding discussions are provided.

### A. Simulation Setup

The simulated scenario is constructed as Fig. 1 shows. The flow of traffic is modeled by a truncated exponential distribution [31]. Under this model, the distance  $l$  between any two adjacent cars satisfies the following distribution:

$$p(l) = \begin{cases} \lambda \cdot \frac{1}{\rho} \exp(-\frac{l}{\rho}) & d_{\min} \leq l \leq d_{\max} \\ 0 & \text{otherwise} \end{cases}, \quad (35)$$

where  $\rho$  is the intensity parameter, and  $\lambda$  is a normalizing coefficient to assure that the integral of  $p(l)$  equals 1. Cars in each lane are assumed to travel at constant velocity, i.e.,  $v_1$  and  $v_2$ , respectively. The detailed scenario settings are shown in TABLE I.

The hyper parameters used in training the Q-networks are shown in TABLE II.

### B. Contrasting Approaches

The first contrasting approach is the random policy, which is to randomly select a subband with equal probability at each time step. The second is a commonly used method in DSA, the myopic policy [32]. The myopic policy aims to

TABLE I  
SCENARIO SETTINGS

Notation	Description	Value
$T$	Time interval between two transmissions (s)	0.1
$P_L$	LRR's transmitting power	Set $\frac{P_L G_t A_e}{4\pi} = 10^4$ ,
$P_S$	SRR's transmitting power	
$A_e$	Effective area	$\frac{P_S G_t A_e}{4\pi} = 10^3$
$G_t$	Antenna gain	
$g$	Decaying coefficient	0.1
$v_1$	Velocity of cars on Lane 1 (m/s)	30
$v_2$	Velocity of cars on Lane 2 (m/s)	-25

TABLE II  
HYPER PARAMETERS IN TRAINING THE Q-NETWORKS

Description	Value		
	Layer	Number of neurons	
network architecture	Input	7	
	FCL	30	
	LSTM1	30	
	LSTM2	30	
	LSTM3	20	
	LSTM4	10	
	Output	$M$	
	batch size $K \times P$	40 × 20	
	exploring probability $\epsilon$	0.05	

select a subband which is most likely to be unused in the next time step. However, it requires prior knowledge of the transition probability of each subband. In [32], a practical realization of the myopic policy is given without knowing the transition probability. To make it more efficient in our multi-radar problem, we make some modifications. In the original myopic policy, all the subbands are kept in an predefined priority order. The user keeps using one subband if the result is a success. Otherwise, it switches to the next subband according to the priority order. In the modified myopic policy, the order is not needed. Radar switches to a random subband when failure occurs. The modified myopic policy outperforms the original version in our problem. Under the modified myopic policy, the subband chosen at time step  $t$  is

$$u_t^i = \begin{cases} u_{t-1}^i & \eta_t^i < \eta_0 \\ \text{a random subband} & \text{otherwise} \end{cases}. \quad (36)$$

### C. Results and Discussions

In Fig. 9, a comparison of the success rate achieved by the three approaches is drawn in two scenarios where  $N = 6, M = 2$  and  $N = 8, M = 3$  ( $M, N$  are the number of subbands and cars), respectively. In the two contrasting approaches, success rate basically does not change with episodes because no learning is involved. The myopic policy performs better than the random policy in both scenarios. In Fig. 9 (a), the average success rate achieved by the myopic and random policy are 58% and 47%; in Fig. 9 (b), they are 58% and 80% and 57%. In the RL-based approach, the success rate increases with episodes and finally becomes stable. In the beginning, the RL-based approach is close to the random policy and outperformed by the myopic policy, because little has been

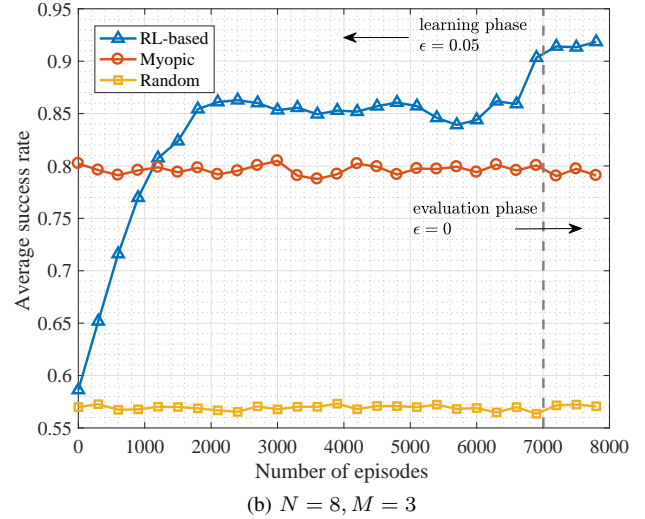
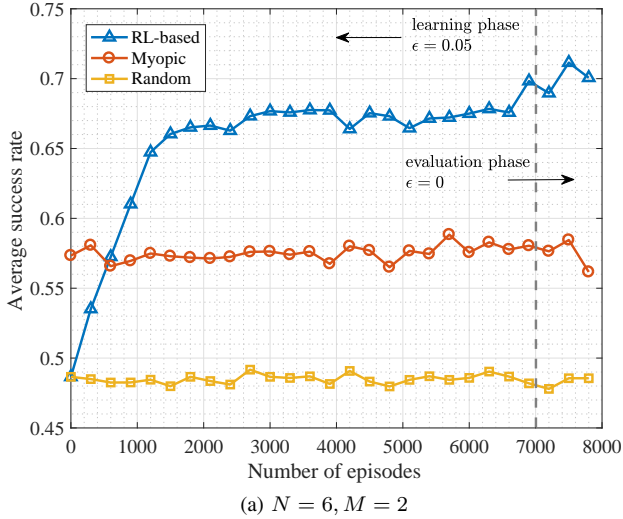


Fig. 9. Success rate of the three approaches versus the number of episodes in two scenarios. The first 7000 episodes correspond to the learning phase, in which  $\epsilon = 0.05$ . The last 1000 episodes correspond to the evaluation phase, in which  $\epsilon = 0.05$ .

learned at first and the exploring probability approximates 1. As the learning proceeds, the RL-based approach quickly surpasses the myopic policy and finally achieves success rate of 70% in Fig. 9 (a) and 90% in Fig. 9 (b), realizing 10% success rate improvement or more over the myopic policy in both scenarios. In Fig. 9, the first 7000 episodes correspond to the learning phase, in which each radar learns but still has 5% probability to randomly choose a subband., i.e. the exploring probability  $\epsilon = 0.05$ . The last 1000 episodes correspond to the evaluation phase, in which each radar chooses subbands strictly according to the learned Q-network, i.e  $\epsilon = 0.05$ . This explains why there is a slight success rate raise in the last 1000 episodes.

In Fig. 10, we compare the final success rate achieved by the three approaches under different scenarios. Each scenario has a different combination of the number of cars and the number of subbands. In each subfigure, the number of cars is fixed and success rate versus the number of subbands is plotted. Generally, success rate achieved by the three approaches all increases with the number of subbands. The RL-based approach has the best performance in all scenarios and the random policy the worst.

In Fig. 11, we plot the success rate improvement by the RL-based approach over the random (Fig. 11 (a)) and myopic policy ( Fig. 11 (b)) versus the number of subbands. In both subfigures, the success rate improvement first increases with the number of subbands and then decreases. Compared with the myopic policy, when there is only one subband, the two approaches equal; then, the improvement reaches its peak at 2 or 3 subbands, mostly exceeding 10%; when there are 5 subbands, the improvement drops below 3%. As the myopic policy is essentially to switch to a random subband when failure occurs, if there are 2 or 3 subbands, the probability of two radars switching to the same subbands is still large (the probability is  $1/M$ ). However, the RL-based approach can use additional position and interference information, processed

by the learned Q-network, to avoid interference. The myopic policy catches up with the RL-based approach when the number of subbands increases because the probability of two radars switching to the same subbands becomes small. By analyzing the improvement of the RL-based approach over the myopic policy, it can be concluded that the RL-based approach is more advantageous when subbands are fewer. This means that using the proposed approach, we can divide the whole band into fewer subbands so that each subband can be allocated with more bandwidth for improving resolution.

Examining the relationship between the performance of the proposed approach and the number of subbands is instructive in dividing the spectrum. As is stated previously, the number of subbands is predefined majorly according to radar resolution or bandwidth requirement. Now, the interference avoidance performance can be another factor to be considered. More subbands guarantee higher success rate but result in lower range resolution due to bandwidth reduction. The proposed approach is verified to be more advantageous over the myopic policy with fewer subbands, which means that we can achieve the same interference avoidance performance with fewer subbands so that each subband can be assigned with more bandwidth for resolution. In other words, our approach makes it more effective to compromise between resolution and success rate.

Furthermore, we verify the robustness of the proposed approach in different road condition, such as the traffic density. In Fig. 12, we plot success rate of the three approaches versus traffic density parameter  $\rho$  under 4 different scenarios. In the RL-based approach, the Q-networks are trained when  $\rho = 0.02$ . Then the trained Q-networks are applied to other cases with values of  $\rho$  ranged from 0.01 to 0.1. Generally, for all three approaches, success rate decreases with the traffic density parameter increasing. Compared to the myopic policy, the RL-based approach has a steady success rate improvement in the examined range of  $\rho$ , which shows that the trained network can be well generalized to other traffic density.

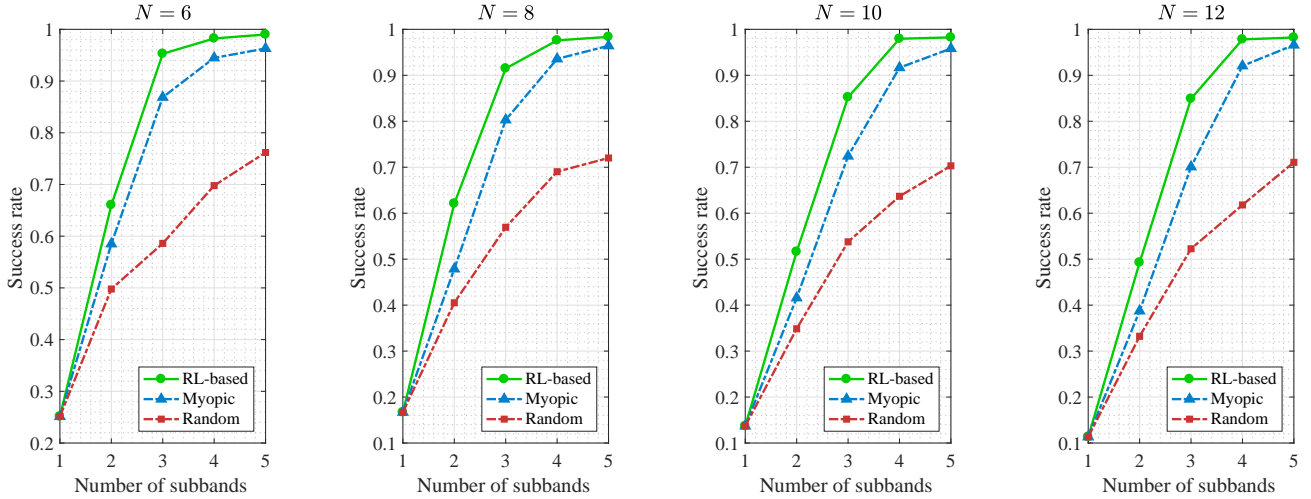


Fig. 10. Success rate achieved by the three approaches versus the number of subbands when the number of cars is fixed.

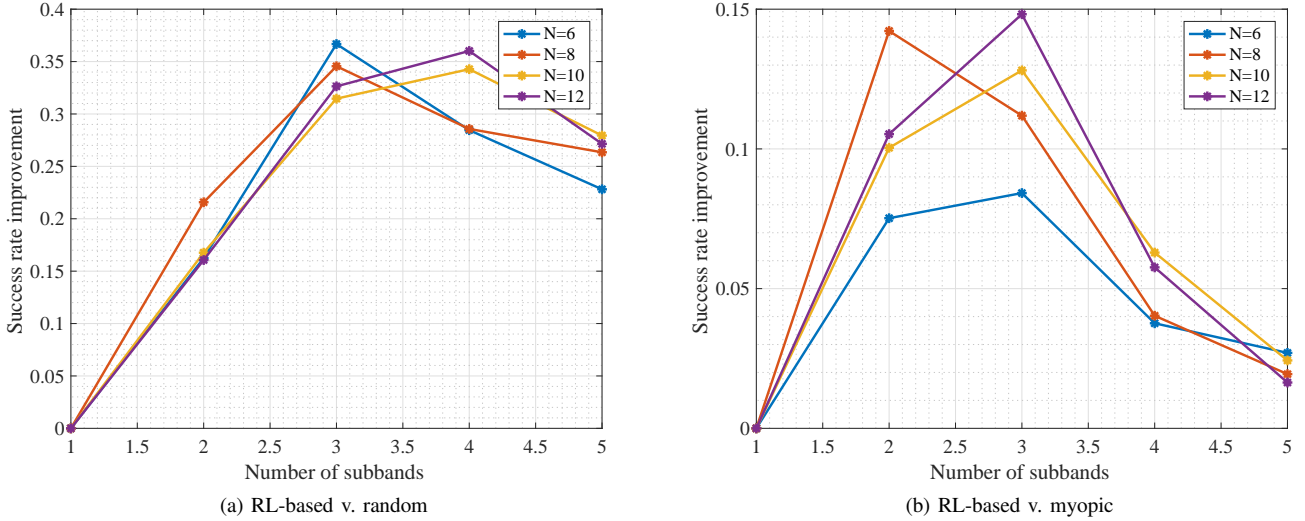


Fig. 11. Success rate improvement by the RL-based approach over the random and myopic policy versus the number of subbands.

## VI. CONCLUSION

In this paper, we study the interference avoiding problem for automotive radar using an RL-based decentralized spectrum allocation approach. With RL, each radar learns to choose a frequency subband merely according to its own observations without communication. Considering radar's single observation is inadequate, an LSTM neural network is incorporated in RL so that a subband is decided by combining both the present and past observations. Simulation experiments are conducted to verify the RL-based approach by comparing it with two commonly used spectrum allocation approaches, i.e., the random and myopic policy. It is shown that the RL-based approach gains a higher success rate improvement than the myopic policy with fewer subbands. Hence, the proposed approach makes it more effective to compromise between resolution and interference.

The simulation model used in this paper is simplified to

demonstrate the feasibility of the proposed approach. Future work will focus on two aspects. One is to construct a simulation model which can better represent the real road environment. The other is to improve the generalization capability of our approach, since now a network is trained and applicable to one specific scenario where the number of cars and the number of subbands are constant. More effort will be put into generalizing our approach for scenarios with variable numbers of cars and subbands.

## REFERENCES

- [1] M. Goppelt, H. L. Blcher, and W. Menzel, "Automotive radar - investigation of mutual interference mechanisms," *Advances in Radio Science*, vol. 8, no. 4, pp. 55–60, 2010.
- [2] G. Kim, J. Mun, and J. Lee, "A peer-to-peer interference analysis for automotive chirp sequence radars," *IEEE*

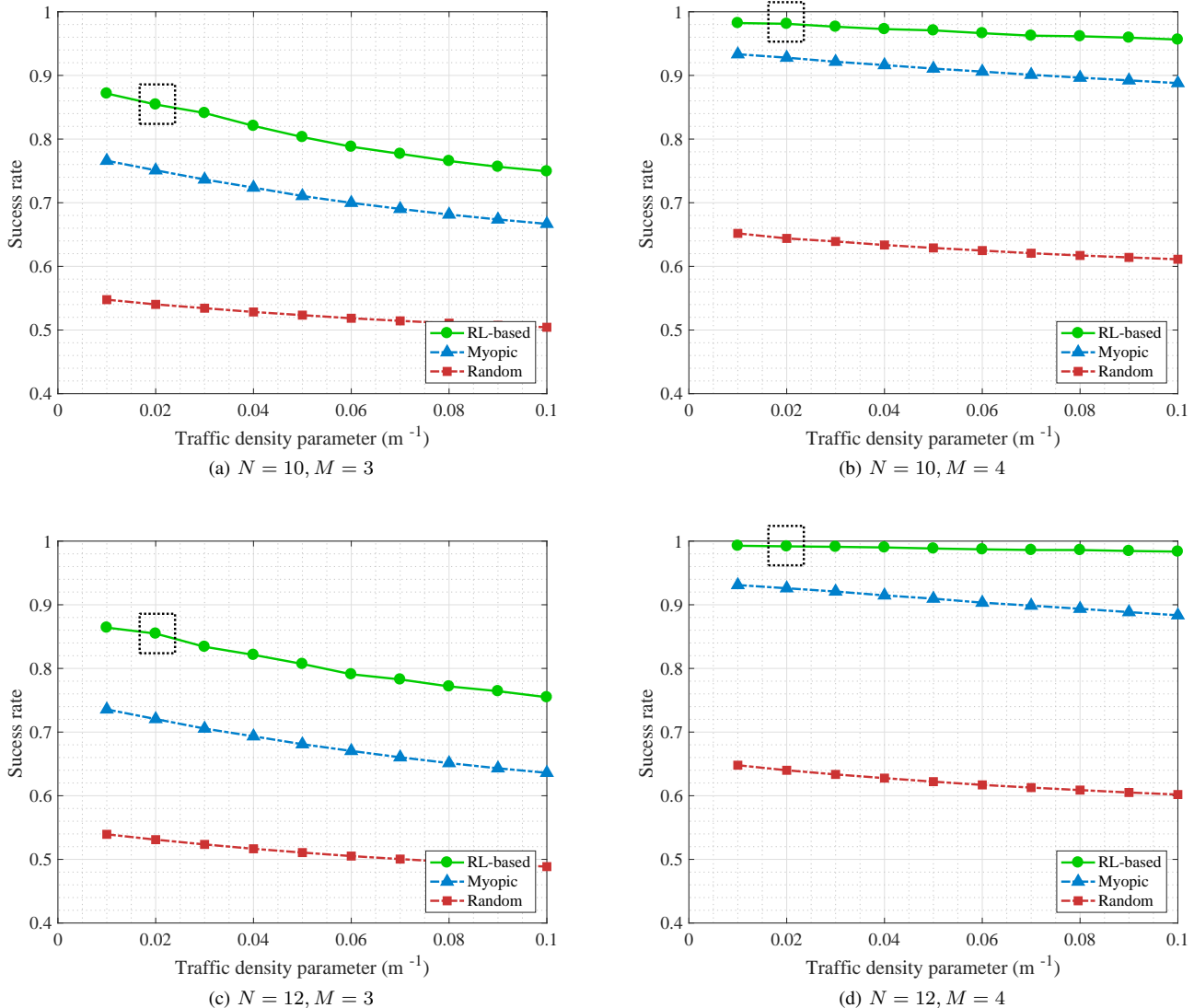


Fig. 12. Success rate achieved by the three approaches versus the traffic density parameter under different scenarios. The dashed box indicates that the Q-networks are trained when the traffic density parameter is 0.02 and then the trained networks are applied to other cases with different traffic density parameter.

*Transactions on Vehicular Technology*, vol. 67, no. 9, pp. 8110–8117, 2018.

- [3] G. M. Brooker, “Mutual interference of millimeter-wave radar systems,” *IEEE Transactions on Electromagnetic Compatibility*, vol. 49, no. 1, pp. 170–181, 2007.
- [4] M. Goppelt, H.-L. Blöcher, and W. Menzel, “Analytical investigation of mutual interference between automotive FMCW radar sensors,” in *2011 German Microwave Conference*. IEEE, 2011, pp. 1–4.
- [5] T. N. Luo, C. H. E. Wu, and Y. J. E. Chen, “A 77-GHz CMOS automotive radar transceiver with anti-interference function,” *IEEE Transactions on Circuits and Systems I Regular Papers*, vol. 60, no. 12, pp. 3247–3255, 2013.
- [6] M. Toth, P. Meissner, A. Melzer, and K. Witrisal, “Analytical investigation of non-coherent mutual FMCW radar interference,” in *2018 15th European Radar Conference*

(*EuRAD*). IEEE, 2018, pp. 71–74.

- [7] M. Kunert, “Project final report,” European Commission: MOre Safety for All by Radar Interference Mitigation (MORARIM), Luxembourg, Tech. Rep. 248231, 2010. [Online]. Available: <https://cordis.europa.eu/project/rcn/94234/reporting/en>
- [8] M. G. Amin, “Interference mitigation in spread spectrum communication systems using time-frequency distributions,” *IEEE Transactions on Signal Processing*, vol. 45, no. 1, pp. 90–101, 1997.
- [9] M. Barjenbruch, D. Kellner, K. Dietmayer, J. Klappstein, and J. Dickmann, “A method for interference cancellation in automotive radar,” in *2015 IEEE MTT-S International Conference on Microwaves for Intelligent Mobility (ICMIM)*. IEEE, 2015, pp. 1–4.
- [10] J. Bechter and C. Waldschmidt, “Automotive radar interference mitigation by reconstruction and cancellation of

- interference component,” in *2015 IEEE MTT-S International Conference on Microwaves for Intelligent Mobility (ICMIM)*. IEEE, 2015, pp. 1–4.
- [11] M. Wagner, F. Sulejmani, A. Melzer, P. Meissner, and M. Huemer, “Threshold-free interference cancellation method for automotive FMCW radar systems,” in *2018 IEEE International Symposium on Circuits and Systems (ISCAS)*. IEEE, 2018, pp. 1–4.
- [12] S. Alland, W. Stark, M. Ali, and M. Hegde, “Interference in automotive radar systems: Characteristics, mitigation techniques, and current and future research,” *IEEE Signal Processing Magazine*, vol. 36, no. 5, pp. 45–59, 2019.
- [13] M. Kunert, F. Bodereau, M. Goppelt, C. Fischer, A. John, T. Wixforth, T. Ossowska, T. Schipper, and R. Pietsch, “D1.5 - study on the state-of-the-art interference mitigation techniques,” European Commission: MOre Safety for All by Radar Interference Mitigation (MORARIM), Luxembourg, Tech. Rep. 248231, 2010. [Online]. Available: <https://cordis.europa.eu/project/rcn/94234/reporting/en>
- [14] J. Khoury, R. Ramanathan, M. C. Dan, R. Smith, and T. Campbell, “RadarMAC: Mitigating radar interference in self-driving cars,” in *IEEE International Conference on Sensing, Communication, and Networking*, 2016, pp. 1–9.
- [15] L. Kang, J. Bo, L. Hongwei, and L. Siyuan, “Reinforcement learning based anti-jamming frequency hopping strategies design for cognitive radar,” in *2018 IEEE International Conference on Signal Processing, Communications and Computing (ICSPCC)*. IEEE, 2018, pp. 1–5.
- [16] L. Wang, S. Fortunati, M. S. Greco, and F. Gini, “Reinforcement learning-based waveform optimization for MIMO multi-target detection,” in *2018 52nd Asilomar Conference on Signals, Systems, and Computers*. IEEE, 2018, pp. 1329–1333.
- [17] S. You, M. Diao, and L. Gao, “Deep reinforcement learning for target searching in cognitive electronic warfare,” *IEEE Access*, vol. 7, pp. 37 432–37 447, 2019.
- [18] H. Li, “Multiagent-learning for aloha-like spectrum access in cognitive radio systems,” *EURASIP Journal on Wireless Communications and Networking*, vol. 2010, no. 1, p. 876216, 2010.
- [19] L. R. Faganello, R. Kunst, C. B. Both, L. Z. Granville, and J. Rochol, “Improving reinforcement learning algorithms for dynamic spectrum allocation in cognitive sensor networks,” in *2013 IEEE Wireless Communications and Networking Conference (WCNC)*. IEEE, 2013, pp. 35–40.
- [20] J. Lunden, S. R. Kulkarni, V. Koivunen, and H. V. Poor, “Multiagent reinforcement learning based spectrum sensing policies for cognitive radio networks,” *IEEE Journal of Selected Topics in Signal Processing*, vol. 7, no. 5, pp. 858–868, 2013.
- [21] O. Naparstek and K. Cohen, “Deep multi-user reinforcement learning for distributed dynamic spectrum access,” *IEEE Transactions on Wireless Communications*, vol. 18, no. 1, pp. 310–323, 2018.
- [22] S. Wang, H. Liu, P. H. Gomes, and B. Krishnamachari, “Deep reinforcement learning for dynamic multichannel access in wireless networks,” *IEEE Transactions on Cognitive Communications and Networking*, vol. 4, no. 2, pp. 257–265, 2018.
- [23] H.-H. Chang, H. Song, Y. Yi, J. Zhang, H. He, and L. Liu, “Distributive dynamic spectrum access through deep reinforcement learning: A reservoir computing-based approach,” *IEEE Internet of Things Journal*, vol. 6, no. 2, pp. 1938–1948, 2018.
- [24] S. Haykin, “Cognitive radar: A way of the future,” *Signal Processing Magazine IEEE*, vol. 23, no. 1, pp. 30–40, 2006.
- [25] J. Hasch, E. Topak, R. Schnabel, T. Zwick, R. Weigel, and C. Waldschmidt, “Millimeter-wave technology for automotive radar sensors in the 77 GHz frequency band,” *IEEE Transactions on Microwave Theory and Techniques*, vol. 60, no. 3, pp. 845–860, 2012.
- [26] H. Rohling, “Radar CFAR thresholding in clutter and multiple target situations,” *IEEE transactions on aerospace and electronic systems*, no. 4, pp. 608–621, 1983.
- [27] R. Sutton and A. Barto, *Reinforcement Learning: An Introduction*. MIT Press, 1998.
- [28] M. Riedmiller, “Neural fitted Q iteration first experiences with a data efficient neural reinforcement learning method,” in *European Conference on Machine Learning*, 2005, pp. 317–328.
- [29] S. Hochreiter and J. Schmidhuber, “Long short-term memory,” *Neural Computation*, vol. 9, no. 8, pp. 1735–1780, 1997.
- [30] M. Volodymyr, K. Koray, S. David, A. A. Rusu, V. Joel, M. G. Bellemare, G. Alex, R. Martin, A. K. Fidjeland, and O. Georg, “Human-level control through deep reinforcement learning,” *Nature*, vol. 518, no. 7540, pp. 529–533, 2015.
- [31] S. Liu, L. Ying, and R. Srikant, “Throughput-optimal opportunistic scheduling in the presence of flow-level dynamics,” *IEEE/ACM Transactions on Networking*, vol. 19, no. 4, pp. 1057–1070, 2011.
- [32] Q. Zhao, B. Krishnamachari, and K. Liu, “On myopic sensing for multi-channel opportunistic access: Structure, optimality, and performance,” *IEEE Transactions on Wireless Communications*, vol. 7, no. 12, pp. 5431–5440, 2008.